Thermodynamic Calculations of Ti Ion Concentrations and Segregation Coefficients during Ti:Sapphire Crystal Growth

Lingling Xuan, Alexander Pisch, Thierry Duffar

Thermodynamic Calculations of Ti Ion Concentrations and Segregation Coefficients During Ti:sapphire Crystal Growth

Lingling Xuan[a], Alexander Pisch[a], Thierry Duffar[a*]

[a]*Univ. Grenoble Alpes, CNRS, Grenoble INP, SIMAP, 38000 Grenoble, France*

**E-mail: thierry.duffar@grenoble-inp.fr*

Abstract

The theoretical phase diagrams of the binary Al_2O_3-Ti_2O_3 and Al_2O_3-TiO_2, as systems calculated using the FactSage™ software and its thermodynamic databases, are re-optimized. This has been performed on the basis of a literature survey on experimental precipitation limits of Ti_2O_3 and TiO_2 in the Al_2O_3 solid solution. The appropriate oxygen partial pressure (p_{O_2}) range for controlling the valence state of Ti ions during Ti:sapphire crystal growth is obtained with respect to the calculated Ellingham type predominance diagram. Factors affecting the p_{O_2} such as furnace gas, crucible material and graphite heating elements are analyzed. The influence of p_{O_2} on Ti^{3+} and Ti^{4+} concentrations in the solid and liquid phases were derived from thermodynamic equilibrium calculations. The equilibrium segregation coefficients of Ti^{3+} and Ti^{4+} in sapphire are calculated to be 0.046 and 0.011, respectively. Taking into account values extrapolated from experiments, a value of 0.06 ± 0.02 is proposed for

the equilibrium segregation coefficient of total Ti under low p_{O_2}.

Key words: Ti:sapphire, Solid solubility, Phase diagram, Oxygen partial pressure, Thermodynamic equilibrium calculations, Segregation coefficient

1 Introduction

Since the large tunable ability from 660 to 1070 nm of Ti:sapphire was discovered by Moulton,[1] these crystals have been receiving great attention from optical experimenters, especially their applications in laser systems such as ultra-short pulse laser generation[2] and high-power amplification.[3] This motivated the crystal growth community to increase the efforts to produce Ti:sapphire crystals with higher optical quality. The reported Ti doping level, for laser applications, ranges from 0.07 to 0.41 mol%.[4] The excellent performance of Ti:sapphire comes from the contribution of doping Ti^{3+} ions. However, whatever the crystal growth method, it is always difficult to eliminate Ti^{4+}ions, that are detrimental to the laser efficiency. Their presence leads to the well-known "residual absorption " resulting from Ti^{3+} - Ti^{4+} pairs.[5] The figure of merit (FOM), which is related to the relative concentration ratio of Ti^{3+}/Ti^{4+}, is used to evaluate the optical quality of Ti:sapphire.[6] The contents of Ti^{4+} could be reduced through annealing but this process is time consuming. Therefore, controlling the valence of Ti ions during Ti:sapphire growth is of critical importance for improving the optical properties of the resulting single crystal.

Crystal growth atmosphere, essentially the partial pressure of oxygen, p_{O_2}, plays an important role in determining the valence of Ti ions.[7,8] The effect of p_{O_2} on Ti ion

valences can be predicted through the Ellingham type predominance diagram. This diagram can be calculated using Gibbs energy minimization software like FactSage,[9] Thermo-Calc[10] or Pandat[11] in combination with optimized thermodynamic databases. Crystal growth occurs under conditions where the Gibbs energy has a minimum value which means a physical or chemical equilibrium is established. Ti:sapphire growth proceeds at high temperature and usually lasts several hours to several weeks and even longer time so that thermodynamic equilibrium can be assumed for the gas phase, liquid phase and solid-liquid interface. Therefore, thermodynamic equilibrium calculations can be performed to obtain some physical or chemical parameters relevant during crystal growth and then gain a deeper understanding of the experimentally observed phenomena.

The influence of oxygen partial pressure p_{O_2} and related effects need to be considered in order to understand the Ti ion valences. Most importantly, the variation of p_{O_2} during the crystal growth influences the Ti ion concentrations in both the solid and the liquid phase and thereby the segregation coefficients. Measured effective segregation coefficients of total Ti (k_{Ti}) in Ti:sapphire were reported from 0.05 to 0.23 (see Table 1). To the best of our knowledge, no one has independently measured the segregation coefficients of Ti^{3+} ($k_{Ti^{3+}}$) and Ti^{4+} ($k_{Ti^{4+}}$), that are key growth parameters for the understanding and control of ion valence distributions in the grown crystal.

The purpose of this contribution is to revisit the Ti:sapphire single crystal growth process using a thermodynamic approach. All presented calculations are performed with FactSage™ software using its thermodynamic databases “FToxid” for

all condensed phases and "FactPS" for the gas species. The thermodynamic data was modified to model the phase diagrams with respect to collected experimental precipitation limits of TiO_2 and Ti_2O_3. The factors influencing p_{O_2} in crystal growth atmosphere are analyzed including filling gas and furnace materials. The influence of oxygen partial pressure on the concentrations of Ti^{3+} and Ti^{4+} in the solid and liquid phases is studied. The segregation coefficients of Ti^{3+}, Ti^{4+} and total Ti are calculated from these results and compared to the experimental values.

Table 1. *Measured Ti effective segregation coefficient in Ti:sapphire grown by different techniques.*

k_{Ti}^{eff}	Crystal growth method	Pulling rate m.s^{-1}	Crucible	Atmosphere	FOM
0.23	Heat exchanger[12]	Unknown	Mo	He	124.6 and 131.2
< 1	Heat exchanger[13]	Unknown	Mo	Vacuum	Unknown
0.2	Kyropoulos[14]	Unknown	Mo	Unknown	Unknown
0.21	Kyropoulos[15]	Unknown	Mo	Vacuum	200
0.2	Kyropoulos[16]	Unknown	Mo	Unknown	Unknown
0.17 - 0.2	Czochralski[17]	2.78×10^{-7}	Ir	Ar/CO	>100
0.12	Czochralski[8]	1.06×10^{-7}	Ir	N_2 or N_2+0.1 vol% H_2	Unknown
0.11	Czochralski[18]	8.47×10^{-8}- 7.06×10^{-7}	Unknown	N_2	Unknown

0.05	Czochralski[19]	2.78×10^{-7}	Ir	N_2	Unknown
0.1	Czochralski[20]	2.78×10^{-7}	Ir	Unknown	Unknown
0.2	μ-pulling down[21]	Unknown	Ir	Ar	Unknown
0.1	Floating zone[22]	Unknown	Mo	N_2 or Ar + 5~20 vol % H_2	Unknown
0.21	Gradient freeze technique[23]	Unknown	Mo	Ar or He	Unknown
0.15	Horizontal directional solidification[24]	1.39×10^{-7}-5.56×10^{-7}	Mo	Ar+5 vol% reductants	>150
0.12 - 0.15	Horizontal directional solidification[25]	1.39×10^{-7}-5.56×10^{-7}	Mo	Ar	Unknown
< 0.2	Unknown[26]	Unknown	Unknown	Unknown	100, ≥150
0.14	Unknown[27]	Unknown	Unknown	Unknown	Unknown
0.1	Unknown[28]	6.94×10^{-8}	Ir	N_2 or Ar	Unknown

2 Literature information on solid solubility and phase diagrams

2.1 Ti ion solubilities in sapphire

Ti:sapphire is usually grown by doping Ti_2O_3 or TiO_2 into alumina raw material. Depending on the crystal growth atmosphere, Ti^{3+} and Ti^{4+} substitution ions are obtained in the sapphire crystal in both cases. However, this process could be accompanied by the formation of precipitates when the solid concentration exceeds the solubility limits of Ti^{3+} and Ti^{4+}. For example, when p_{O_2} is high, precipitates such as

rutile (TiO_2) may form inside the crystal. When p_{O_2} is low, most Ti^{4+} ions are reduced to Ti^{3+} and Ti_2O_3 precipitates could form. Therefore, the solubilities of Ti^{3+} or Ti^{4+} are critically important. A thorough assessment of the underlying phase diagram is necessary and will be used to compute Ti ion concentrations and segregation coefficients.

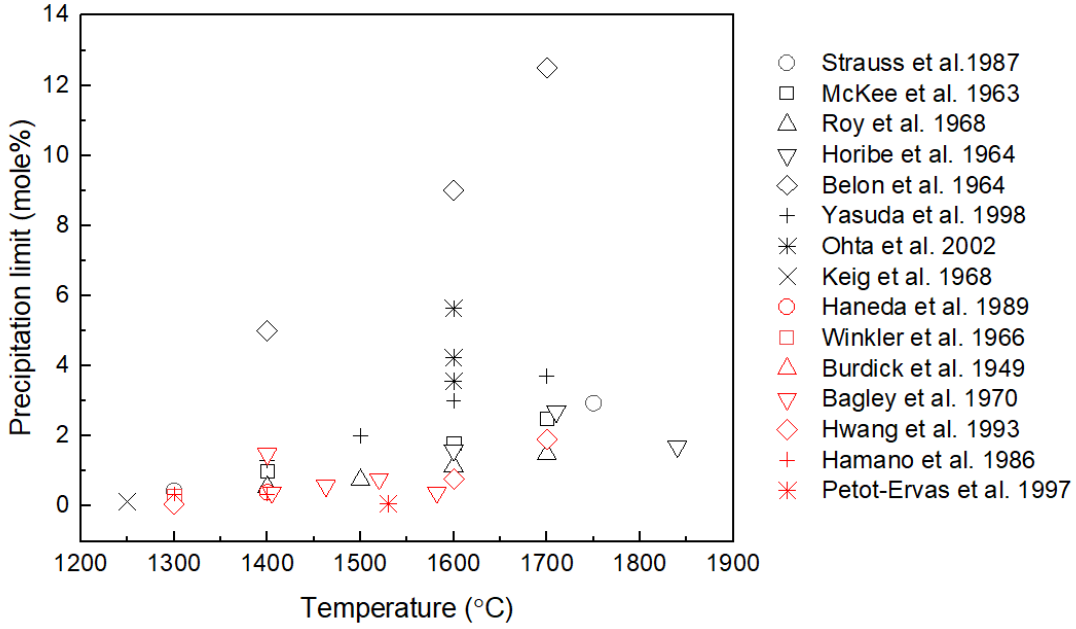

Figure 1. *Solid precipitation limit of Ti_2O_3 and TiO_2 in α-Al_2O_3. Black symbols represent the precipitation limit of Ti_2O_3 and red symbols represent the precipitation limit of TiO_2.*[23,29–42]

The reported solid solubilities of Ti^{3+} and Ti^{4+} in alumina are summarized in Figure 1. Both solubilities of Ti^{3+} and Ti^{4+} increase with elevating temperature. It is observed that Ti^{3+} is more soluble in α-Al_2O_3 than Ti^{4+}. This is reasonable because no extra charge compensator is required for the incorporation of Ti^{3+} while one aluminum vacancy is created together with the incorporation of every three Ti^{4+} to maintain

electroneutrality.

There may exist some uncertainties for part of the solubility data. For example, under reducing atmosphere, Ti^{3+} should be expected while Roy et al. ascribed their obtained solubility data to Ti^{4+}.[40] The solubility of Ti^{4+} given by Winkler et al. is measured in polycrystalline Al_2O_3, not in a single crystal.[34] Even though, their results are still considered as a reference by most researchers. Ohta et al. measured the solubility of Ti^{3+} in Al_2O_3 at 1600 ℃ in the ternary Al_2O_3-SiO_2-TiOx system but not in the pure Al_2O_3-Ti_2O_3 system.[31] For papers where p_{O_2} is not known, it is assumed that Ti^{3+} solid solubilities were obtained under reducing atmosphere (low p_{O_2}) and Ti^{4+} solid solubilities were obtained under oxidizing atmosphere (high p_{O_2}). These experimental solubility data will be further discussed under the following phase diagrams.

2.2 Al_2O_3-Ti_2O_3 and Al_2O_3-TiO_2 quasi-binary systems

Under reducing atmosphere, the major fraction of titanium in the system is present as Ti^{3+}. The calculated phase diagram of Al_2O_3-Ti_2O_3 system at p_{O_2} =10^{-15} bar accompanied by the experimental solubility data of Ti^{3+} from the literature is shown in Figure 2, as calculated using FastSage 8.0 software. It is assumed that no metal phase (Al, Ti, TiAl, $TiAl_3$ …) is formed in the solid phase. The solidus and solvus lines of Al_2O_3 show a good agreement with the Ti^{3+} solid solubility data in Figure 2 except the results of Belon et al which reported a precipitation limit of Ti_2O_3 in Al_2O_3 as high as 12.5 mole% at 1700 ℃.[42] All other reported precipitation limits of Ti_2O_3 in Al_2O_3 are

lower than 4 mole%. Except Ti_2O_3 (ilmenite-type phase), several other titanium oxides, Magnéli phases (Ti_nO_{2n-1}, $4 \leq n \leq 20$), are also present in the quasi-binary Al_2O_3-Ti_2O_3 system. These Magnéli phases are considered as stoichiometric compounds in the temperature range 1200 – 1300 °C.[43]

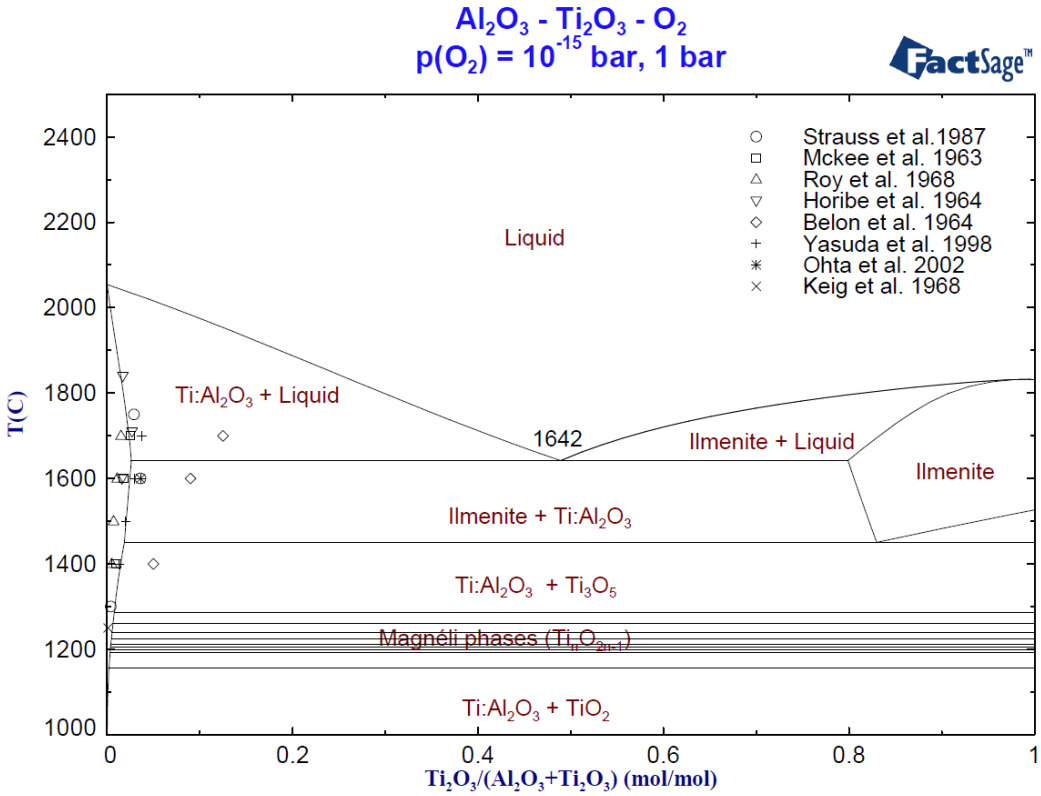

Figure 2. *Phase diagram of quasi-binary Al_2O_3-Ti_2O_3 system at fixed oxygen partial pressure of $p_{O_2} = 10^{-15}$ bar and $p_{total} = 1$ bar.*[23,29–32,40–42]

The calculated phase diagram of the quasi-binary Al_2O_3-TiO_2 system in air, zoomed on the low Ti concentration range, is shown in Figure 3. The solubility data of Ti^{4+} from the literature are plotted together with the calculated phase boundaries. According to FactSage result, titanium ions are totally incorporated into Ti:sapphire for low concentrations only (in the left small area of Figure 3). However, the experimental

solubility data does not agree with the calculated phase diagram. This is due to the fact that, in the commercial FactSage software and its databases, the solubility data of Ti^{4+} in the Al_2O_3 solid phase is neglected and not modelled. The calculated solubility of Ti in Al_2O_3 in Fig.3 is due to Ti^{3+} ions only. It is therefore impossible to calculate the equilibrium concentrations of Ti^{3+} and Ti^{4+} in the solid phase and to determine the corresponding segregation coefficients. Therefore, the solid database must be optimized to reproduce the experimental solubility data for Ti^{3+} and Ti^{4+} ions.

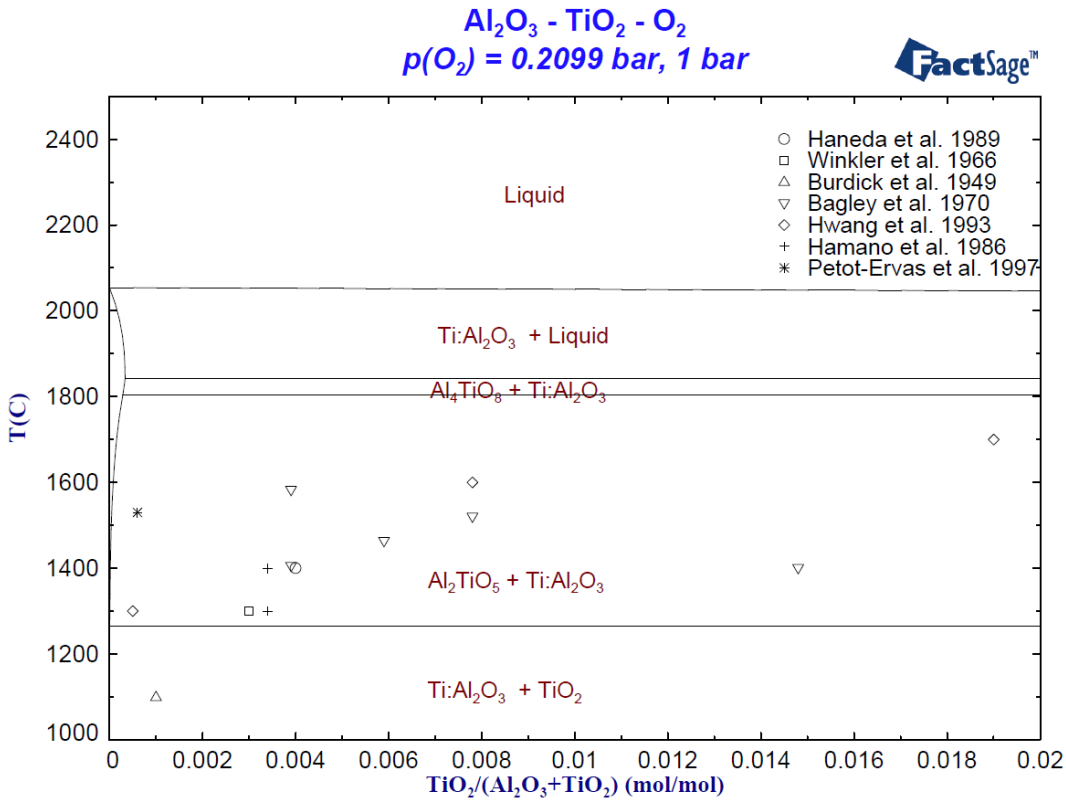

Figure 3. *Zoomed phase diagram of the Al_2O_3-TiO_2 system in air and* $p_{total} = 1$ *bar.*[33–39]

To improve the database for the thermodynamic equilibrium calculations, Ti^{4+} ions can be introduced into the solid phase by adding TiO_2 as diluted component into

the solid solution through the Henrian relation given as:

$$\log_{10} \gamma_i = \frac{A}{T} + B \qquad (1)$$

where γ_i is the dimensionless activity coefficient of Ti^{4+}, A and B are constants, T is the temperature in Kelvin. The solidus and solvus lines in quasi-binary Al_2O_3-TiO_2 phase diagram change with A, B parameters and with the oxygen partial pressure p_{O_2}. The thermodynamic data of pure TiO_2 (rutile) from the FTPS pure substance database[9] was selected as diluted component in the modelling of the Ti:Al_2O_3 solid solution to calculate realistic Al_2O_3-TiO_2 equilibria at high temperature. By dichotomy, it was found that A= 4360 and B=0 result in an acceptable fit of the phase diagram with the experimental solubility data.

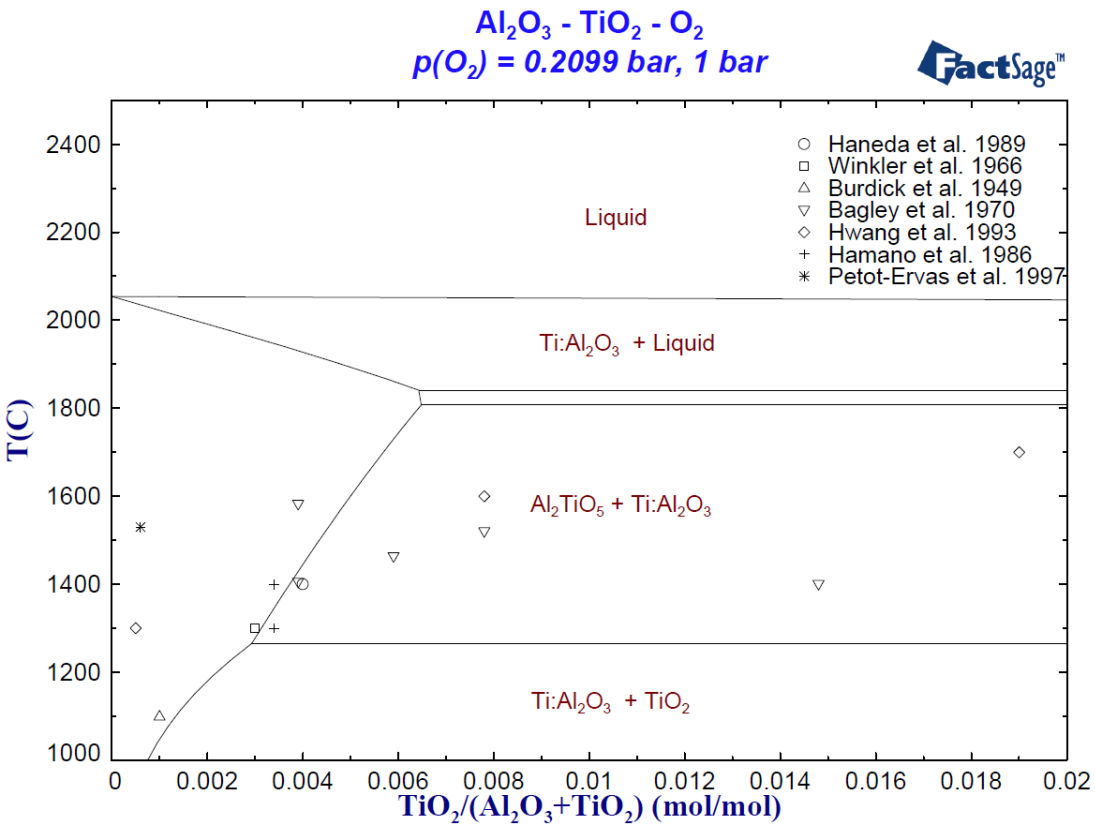

Figure 4. *Optimized phase diagram of Al_2O_3-TiO_2 system in air after imported Ti^{4+} into the solid phase and $p_{total} = 1$ bar.*

The new phase diagram of Al_2O_3-TiO_2 with the diluted solution is presented in Figure 4 along with the experimental solubility data of Ti^{4+} ions. Compared to Figure 3, the solubility data of Ti^{4+} distributes well on the solvus line. The phase diagram of Al_2O_3-Ti_2O_3 system has nearly no change compared to the initial diagram. This new modified thermodynamic database is used for all further calculations presented in this contribution.

The valence of Ti in the crystal is a function of temperature and oxygen partial pressure. An important point to mention is that there exist large temperature differences in a crystal growth setup. For example, in Kyropoulos and Czochralski crystal growth setups, the temperature of the crucible wall is higher than that in the center of the melt and the temperature on the earlier grown part (top of the crystal) is lower than the temperature of the bottom part which is close to the solid-liquid interface. The temperature varies also drastically during crystal cooling process. Therefore, for the aim of getting the desired valence of Ti^{3+}, oxygen partial pressures must be carefully controlled to fit the phase diagram at any temperature. At high temperature, it is possible that O_2 gas is decomposed into O atoms, but from the experimental aspect, p_{O_2} has much more physical meaning than p_O and it is easier to compare the results with experiments. Therefore, in the thermodynamic calculations, p_{O_2} is used to describe the oxygen partial pressure.

Based on the optimized database, an Ellingham type predominance diagram of the Al_2O_3-TiO_2 system (see Figure 5) can be calculated and shows the relation of the oxygen partial pressure p_{O_2} with temperature as well as its influence on the Ti ion

valence. The Al_2O_3 solid solution, "Ti:Al_2O_3" and the ionic "Liquid" coexist at high temperature. The solid phase containing Ti^{3+} and Ti^{4+} ions, without the precipitation of other phase, exists only within the shaded area (Ti:Al_2O_3). So, in order to grow this solid solution, the oxygen partial pressure p_{O_2} should be higher than 10^{-20} bar. At high temperature (T >1000 °C), for p_{O_2} lower than 10^{-20} bar, TiO may appear. At low temperature (T < 1000 °C), rutile (TiO_2) precipitates may form in the crystal. It has been observed in the sintering experiments of Hamano et al., that excess TiO_2 precipitates as rutile at temperatures below 1350 °C.[38]

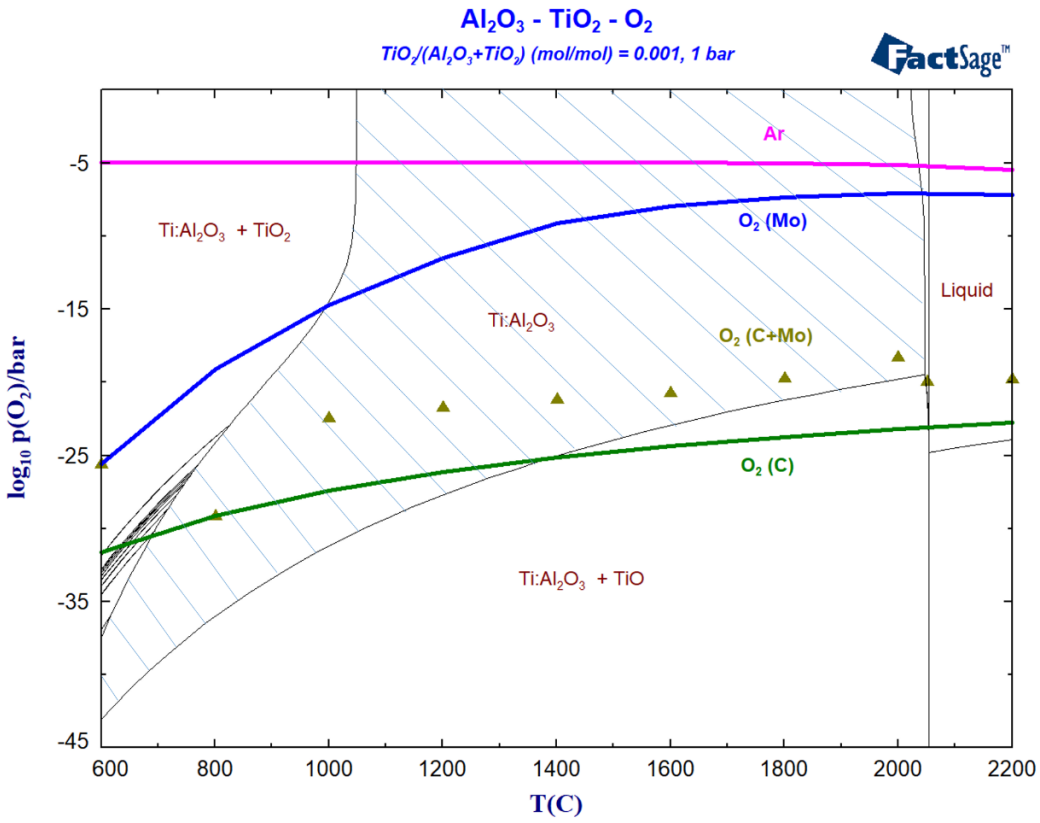

Figure 5. *Ellingham type predominance diagram of the Al_2O_3-TiO_2 system. "Ar" shows the p_{O_2} for Ar + 10 ppm O_2 +10 ppm H_2O; "O_2 (Mo)" shows the p_{O_2} for Ar + 10 ppm O_2 +10 ppm H_2O in equilibrium with Mo; "O_2 (C)" shows the p_{O_2} for Ar +*

10 ppm O_2 +10 ppm H_2O in equilibrium with graphite elements; "O_2 (C+Mo)" (gray triangles) shows the p_{O_2} for the two steps calculation with C and Mo (see text).

3 p_{O_2} during Ti:sapphire growth

The oxygen partial pressure inside the furnace at any time is conditioned by the crystal growth conditions (temperature, atmosphere, crucible, furnace structure and materials). For example, Figure 6 shows a simplified sketch of a setup used for growing Ti:sapphire using the Kyropoulos method. The crystal is grown under flowing Ar gas.

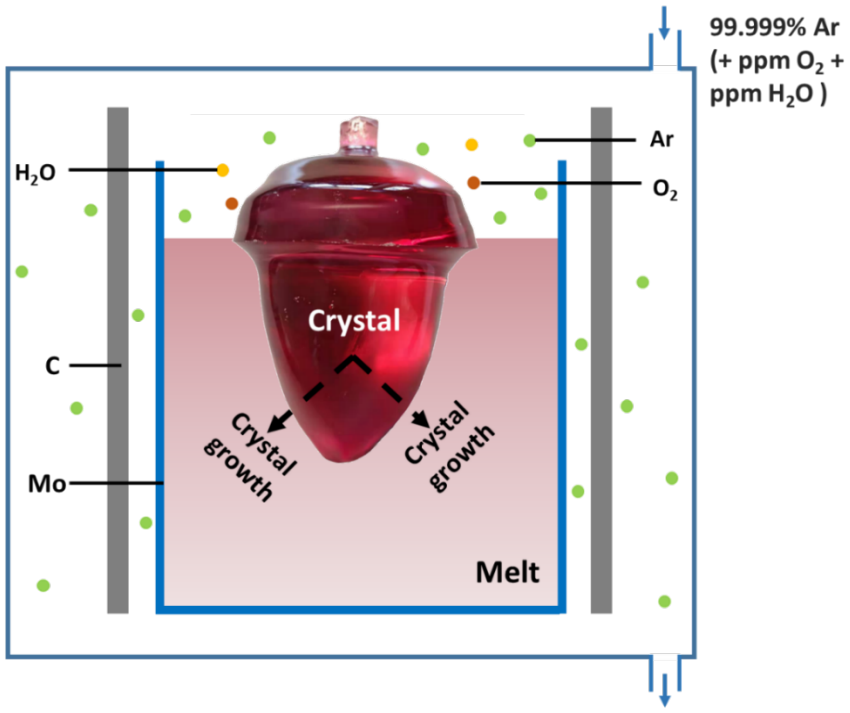

Figure 6. *Kyropoulos crystal growth sketch for Ti:sapphire. The inserted crystal picture has been obtained by extracting a crystal from the melt during growth.*[44]

But, even the purest commercial Ar gas always contains small amounts of dioxygen (O_2) and water vapor. In addition, the furnace cannot be perfectly sealed. Small amounts of dioxygen and water vapor leaking in from the ambient air still have a chance to enter

in the furnace. Thus, it is assumed that 10 ppm O_2 and 10 ppm H_2O (g) trace impurities are present inside the flowing furnace gas.[17] The raw material, composed of pure alumina crackles and Ti doped Al_2O_3 powder, is melted in a metallic Mo crucible and the crystal is grown along radial and downward directions. Graphite elements are used as casing, susceptor and insulation for uniformly heating the crucible. The gas (initially Ar + 10 ppm O_2 + 10 ppm H_2O (g)) exists everywhere inside the furnace.

Except for specific study purposes, Ti:sapphire is always grown under pure inert gas or reducing gas to obtain a sufficient concentration of Ti^{3+} ions for an application in laser materials. Reported Ti:sapphire crystals were grown under pure Ar, N_2, and H_2 atmospheres.[45,46] In contrast to pure inert gases, mixtures of inert gas with small amounts of reducing gas in the growth or annealing processes contribute to further improve crystal quality. It is already reported that Ti:sapphire grown under the mixtures of 99.34 % Ar + 0.6% CO + 0.06 % H_2 can lower the $[Ti^{4+}]/[Ti^{3+}]$ ratio.[47] The results of Uecker et al. suggest that the mixtures of 95% Ar + 5% CO is efficient in maintaining titanium ions at the +3 valency.[17]

Mo, W and Ir metals are three typical crucible materials used in Ti:sapphire crystal growth. Trace impurities of O_2 and H_2O (g) in the growth atmosphere can oxidize the crucible metal through below reactions:[48,49]

$$Mo(s) + O(g) \rightarrow MoO(g)$$

$$2Mo(s) + 3O_2(g) \rightarrow 2MoO_3(g)$$

$$Mo + 2H_2O \leftrightarrow MoO_2 + 2H_2$$

$$MoO_2 + H_2O \leftrightarrow MoO_3 + H_2$$

$$\mathrm{W(s) + O_2(g) \leftrightarrow WO_2(s)}$$

$$\frac{2}{3}\mathrm{W(s) + O_2(g) \leftrightarrow \frac{2}{3}WO_3(s)}$$

$$\mathrm{Ir(s) + O_2(g) \leftrightarrow IrO_2(s).} \quad (2)$$

These produced oxides are volatile so that the crucible is decomposed and destroyed when the oxygen partial pressure p_{O_2} is too high. In the liquid phase, it is calculated that the potential reaction among alumina melt, crucible materials and furnace gas leads to the lowest oxygen partial pressure of 8.87×10^{-8} bar at sapphire melting point for Mo crucible while W crucible gives a $p_{O_2} = 4.27 \times 10^{-7}$ bar and Ir crucible gives a $p_{O_2} = 6.22 \times 10^{-6}$ bar, respectively. Besides, Ir is expensive and W is rather difficult to machine, especially for the small die pieces used for the EFG (Edge-defined Film-fed Growth) process. Therefore, Mo crucible is favored by industrial crystal growers as well as the RSA le Rubis SA company providing us samples. Sometimes, a Mo crucible is used without graphite insulation. In this case, Al_2O_3 or ZrO_2 casings are used. Without Mo crucible (only Al_2O_3 + gas), an oxygen partial pressures p_{O_2} of 6.22×10^{-6} bar is obtained. This means that even with a casing made of oxides, the Mo crucible still controls the p_{O_2} in the liquid phase. It may also be possible that oxygen in the melt or gas diffuses through the Mo crucible but this is not considered in the present study.

However, most of the time, graphite casing is used. The graphite elements inside the furnace also can react with O_2 (g) and H_2O (g):

$$\mathrm{C + \frac{1}{2}O_2 \leftrightarrow CO}$$

$$\mathrm{C + O_2 \leftrightarrow CO_2}$$

$$\mathrm{\frac{1}{2}C + \frac{1}{2}CO_2 \leftrightarrow CO}$$

$$CO + \frac{1}{2}O_2 \leftrightarrow CO_2$$

$$C + H_2O \leftrightarrow CO + H_2$$

$$C + 2H_2O \leftrightarrow CO_2 + 2H_2$$

$$C + 2H_2 \leftrightarrow CH_4 \quad (3)$$

As the Factsage Gibbs energy minimization software calculates the global equilibrium, all these reactions are considered automatically while establishing the final thermodynamic equilibrium under a given set of constraints (temperature, pressure, composition).

In a practical crystal growth run, the gas inside furnace reacts with Mo and graphite in a complex way and at different temperatures. As shown in the crystal growth setup (Figure 6), the crucible is located at the center of the furnace and is surrounded by the graphite elements. So, it is expected that the filling gas reacts first with the outer graphite elements and then reacts later with the central crucible. Consequently, the p_{O_2} around crystal and melt at a given temperature is computed in two steps: 1st, the gas inside furnace reacts with graphite elements; 2nd the resulting gases react with Mo crucible.

To observe the influence of the growth atmosphere on the Ti valence during Ti:sapphire growth, various computed oxygen partial pressures p_{O_2} are plotted in the Al_2O_3-TiO_2 predominance diagram (Figure 5). The plots show that pure Ar gas (pink line) always results in an oxygen partial pressure p_{O_2} of around 10^{-5} bar with no significant change with temperature: there is a risk of TiO_2 precipitation below 1100°C. The successive reactions of C, then Mo (gray triangles, several temperatures are

computed) decrease the oxygen partial pressure p_{O_2} by 13 orders of magnitude compared to Mo action alone (blue line). However, when furnace gases react only with C (green line), it results in the formation of TiO precipitates for temperatures larger than1400 °C instead of forming the pure Al_2O_3 solid solution where only Ti^{3+} and Ti^{4+} exist. It is then concluded that the presence of the Mo crucible, close to liquid and crystal, is likely to suppress the formation of TiO precipitates.

The successive effects of C and Mo results in an oxygen partial pressure $p_{O_2} = 1.1 \times 10^{-20}$ bar that allows growing the desired Ti^{3+} and Ti^{4+} solid solution. During the cooling process, the p_{O_2} partial pressure must be further decreased, otherwise solid rutile (TiO_2) precipitates may appear. Therefore, p_{O_2} must be carefully controlled during the crystal growth and the cooling process. If it is considered that precipitation is a slow process below 1000 °C, growth in presence of C+Mo or even Mo alone are acceptable situations for obtaining crystals without solid precipitates.

4 Ti ion concentrations and segregation coefficients

4.1 Ti ion concentrations

The p_{O_2} partial pressure in the gas phase affects the Ti valence during the crystal growth and as a consequence the concentrations of Ti^{3+} and Ti^{4+} ions present in the crystals. For a sapphire crystal doped with 0.1 mole% TiO_2, the concentrations of Ti^{3+} and Ti^{4+} in the solid and liquid phases at the solid-liquid equilibrium (2053 °C), are computed as function of p_{O_2} partial pressure (Figure 7), based on the previously optimized database.

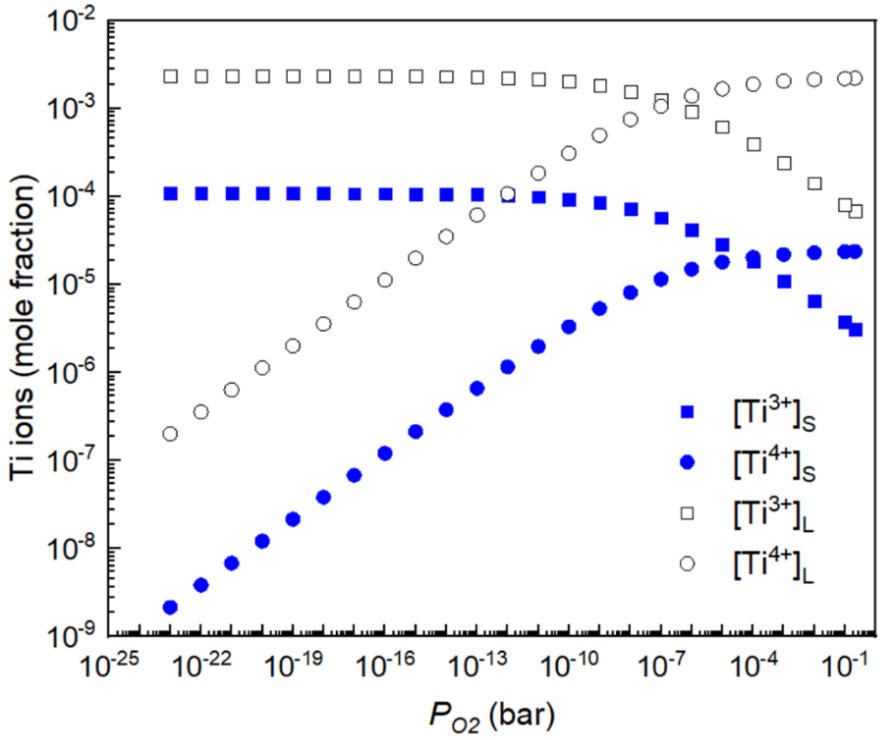

Figure 7. *Ti ion concentrations in the Al_2O_3 solid solution in equilibrium with the liquid and their dependence on p_{O_2} at 2053 °C. The data are calculated from 1mole Al_2O_3 + 10^{-3} mole TiO_2 + 1 mole Ar + appropriate amount of O_2 under fixed p_{O_2}.*

In the liquid phase, when the fixed p_{O_2} partial pressure is smaller than 10^{-7} bar, Ti^{3+} concentration is larger than the concentration of Ti^{4+} while above this pressure, Ti^{4+} concentration becomes the larger one. In the solid phase, the concentration of Ti^{4+} becomes larger than Ti^{3+} when $p_{O_2} > 1\times10^{-4}$ bar. Mohapatra et al. also observed this reverse concentration phenomenon by annealing Ti:sapphire crystals at 1600 °C under different atmospheres.[50] Therefore, when a crystal is grown or annealed under a given temperature, desired Ti ion concentrations can be adjusted through carefully controlling the oxygen partial pressure p_{O_2}. In addition, when the p_{O_2} partial pressure is low ($p_{O_2} < 10^{-20}$ bar), the presence of Ti^{4+} ions still can be observed. When p_{O_2} is high, e.g. 1

bar, the concentration of Ti^{3+} ions is only one-order of magnitude lower than the Ti^{4+} ions so that its concentration cannot be neglected. Therefore, no matter whether the p_{O_2} partial pressure is very high or very low, Ti^{3+} and Ti^{4+} ions always co-exist in grown crystals. Consequently, most reported empirical formula[51,52] used to estimate the concentrations of Ti^{3+} and Ti^{4+} through the absorption coefficient and cross section are not reliable because all these formulas are obtained on the assumption that "only Ti^{3+}" or "only Ti^{4+}" ions exist in the calibration crystal.

4.2 Ti ion segregation coefficients

Ti has a segregation coefficient lower than unity in sapphire (see Table 1) resulting in more Ti remaining in the melt than incorporated into the crystal. This is consistent with Figure 7, i.e. $[Ti^{3+}]_L > [Ti^{3+}]_S$ and $[Ti^{4+}]_L > [Ti^{4+}]_S$. The segregation coefficients of Ti ions are defined as the ratio of Ti ion concentration in the solid phase to the concentration in the liquid phase:

$$k_{Ti^{3+}} = \frac{[Ti^{3+}]_S}{[Ti^{3+}]_L}, \quad (4)$$

$$k_{Ti^{4+}} = \frac{[Ti^{4+}]_S}{[Ti^{4+}]_L}. \quad (5)$$

It is important to mention that the total Ti segregation coefficient does not equal the sum of the segregation coefficients of Ti^{3+} and Ti^{4+} but is described as:

$$k_{Ti} = \frac{[Ti^{3+}]_S + [Ti^{4+}]_S}{[Ti^{3+}]_L + [Ti^{4+}]_L}. \quad (6)$$

According to the Ti ion concentrations shown in Figure 7, the segregation coefficients of Ti^{3+}, Ti^{4+} and total Ti at 2053 ℃ are computed and are presented in Figure 8. It is found that $k_{Ti^{3+}} > k_{Ti} > k_{Ti^{4+}}$.

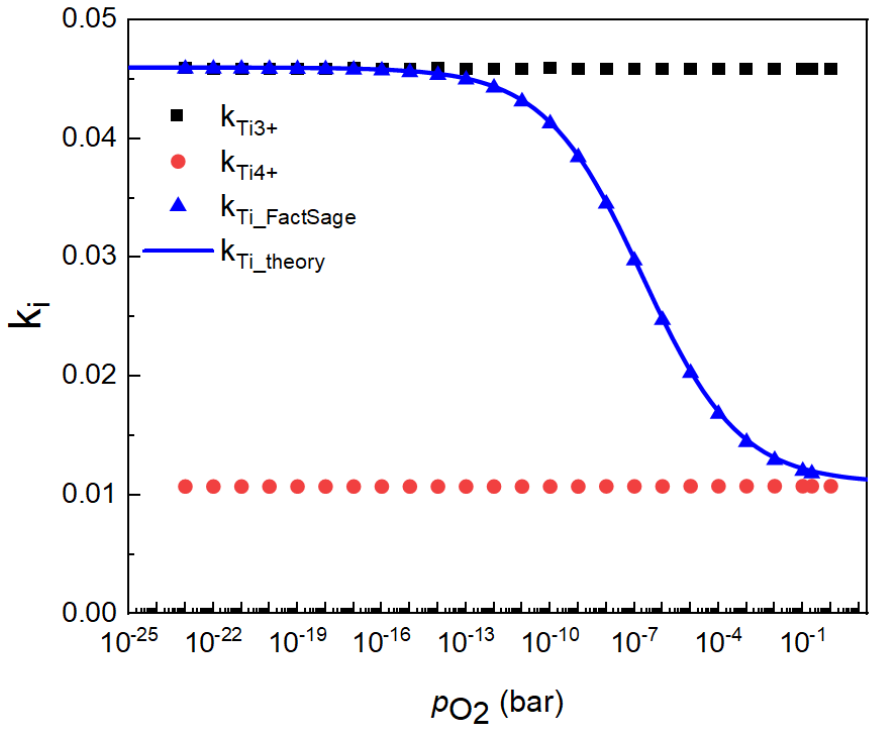

Figure 8. *Ti segregation coefficients dependence on* p_{O_2} *at 2053 ℃.* k_{Ti_theory} *is calculated by Eq.(14).*

When the oxygen partial pressure p_{O_2} is very small (reducing atmosphere), most Ti is present as Ti^{3+}. It follows from equation (6) that

$$k_{Ti} = \frac{[Ti^{3+}]_s + [Ti^{4+}]_s}{[Ti^{3+}]_L + [Ti^{4+}]_L} \approx \frac{[Ti^{3+}]_s}{[Ti^{3+}]_L} = k_{Ti^{3+}}. \quad (7)$$

Similarly, when the partial pressure p_{O_2} is very high (oxidizing atmosphere), most Ti is present as Ti^{4+}. Then k_{Ti} can be approximated as

$$k_{Ti} = \frac{[Ti^{3+}]_s + [Ti^{4+}]_s}{[Ti^{3+}]_L + [Ti^{4+}]_L} \approx \frac{[Ti^{4+}]_s}{[Ti^{4+}]_L} = k_{Ti^{4+}}. \quad (8)$$

Therefore, the increase of p_{O_2} leads to k_{Ti} decreasing gradually from the maximum value $k_{Ti^{3+}} = 0.046$ to the minimum value $k_{Ti^{4+}} = 0.011$. This can be seen on Figure 8. The variation of p_{O_2} has no significant effect on $k_{Ti^{3+}}$ and $k_{Ti^{4+}}$: a variation lower than 0.5% is found from 10^{-20} to 10^{-1} bar.

Defining the ratio of $[Ti^{4+}]$ and $[Ti^{3+}]$ in the liquid phase as

$$\frac{[\mathrm{Ti}^{4+}]_{\mathrm{L}}}{[\mathrm{Ti}^{3+}]_{\mathrm{L}}} = \alpha, \tag{9}$$

it can be written as

$$\alpha = K_{eq} \cdot p_{\mathrm{O}_2}^{\frac{1}{4}}, \tag{10}$$

where K_{eq} is the equilibrium constant of the simplified liquid phase reaction:

$$\mathrm{TiO}_{1.5} + \frac{1}{4}\mathrm{O}_2 \leftrightarrow \mathrm{TiO}_2, \tag{11}$$

with K_{eq} as:

$$K_{eq} = \frac{[\mathrm{TiO}_2]}{[\mathrm{TiO}_{1.5}] \cdot p_{O2}^{\frac{1}{4}}} = \exp\left(-\frac{\Delta G^{\circ}}{RT}\right), \tag{12}$$

where ΔG^0 is the standard molar Gibbs energy given by FactSage database:

$$\Delta G^{\circ} = -202.262 + 0.055 \cdot T \ (\mathrm{kJ.mol^{-1}}). \tag{13}$$

At 2053 ℃, the Gibbs energy of reaction (11) is calculated to be -74.86 $\mathrm{kJ.mol^{-1}}$ using the "Reaction" module in FactSage. It follows from equations (6), (9), (10) and (12) that the theoretical value for the segregation coefficient of total Ti is:

$$k_{\mathrm{Ti\_theory}} = \frac{k_{\mathrm{Ti}^{3+}} + 48 \cdot k_{\mathrm{Ti}^{4+}} \cdot p_{\mathrm{O}_2}^{1/4}}{1 + 48 \cdot p_{\mathrm{O}_2}^{1/4}}. \tag{14}$$

The relation between $k_{\mathrm{Ti\_theory}}$ and p_{O_2} is also plotted in Figure 8. It is found that the thermodynamically calculated $k_{\mathrm{Ti\_FactSage}}$ is very close to the theoretical deduction $k_{\mathrm{Ti\_theory}}$. This shows that the theoretical expression, based on the simplified reaction (11), gives useful accurate values.

Experimentally measured effective segregation coefficients for total Ti are sometimes referred as Ti^{3+} segregation coefficient,[14] based on the assumption that all Ti is present as Ti^{3+} and nearly no Ti^{4+} is present in the crystal. But in a practical crystal growth process, there are always Ti^{4+} ions present in the grown crystals, as shown by

the results on Fig 7. It is noted that the calculated $k_{\mathrm{Ti}^{3+}}$ is much smaller than reported experimental values listed in Table 1. This is because the measured experimental values are the effective segregation coefficient for total Ti while the calculated values are thermodynamic equilibrium segregation coefficients of Ti^{3+}. Additionally, the reported values vary upon crystal growth techniques and conditions, depending on rotation and pulling rates. It was shown that a slow growth rate and rotation rate tend to increase the segregation of dopants, while fast growth rate and rotation rate tend to decrease dopant segregation.[53] So, the exact thermodynamic segregation coefficients of Ti^{3+}, Ti^{4+} and Ti, cannot be determined directly from experiments. Further, the segregation experiments in the literature show that the effective segregation coefficient is necessarily larger than the thermodynamic one ($k_0 < k_{eff} < 1$).

There are very few papers discussing the equilibrium segregation coefficient of Ti and its relationship with growth and rotation rates. According to the well-known Burton, Prim, Slichter (BPS) equations and boundary layer thickness (δ) for the Czochralski crystal growth process:[54,55]

$$\delta = 1.6 D_L^{1/3} \nu_{\mathrm{viscosity}}^{1/6} \omega^{-1/2}, \tag{15}$$

$$k_{Ti}^{eff} = \frac{k_0}{k_0 + (1-k_0) e^{-(V_{\mathrm{growth}} \delta / D_L)}},$$

it is obtained that

$$k_{Ti}^{eff} = \frac{a}{a + (1-a) e^{-(b \times V_{\mathrm{growth}})}}, \tag{16}$$

where $D_L = 5 \times 10^{-9}\ \mathrm{m^2.s^{-1}}$ is the diffusion coefficient of Ti in the liquid alumina, $\nu_{\mathrm{viscosity}} = 1.9 \times 10^{-5}\ \mathrm{m^2.s^{-1}}$ is the kinematic viscosity of the alumina melt,[56] ω is the rotation rate, $a = k_0$ and $b = 1.6 D_L^{\frac{-2}{3}} \nu_{\mathrm{viscosity}}^{\frac{1}{6}} \omega^{\frac{-1}{2}}$. This equation describes the relation between the effective segregation coefficient and the corresponding crystal growth and rotation rates.

Table 2. *Effective segregation coefficient of Ti measured in Ti:sapphire grown by the Czochralski process under different growth and rotation rates.*

k_{Ti}^{eff}	Pulling rate ($m.s^{-1}$)	Rotation rate (min^{-1})
0.17-0.20[17]	2.78×10^{-7}	10-15[57]
0.12[8]	1.06×10^{-7}	5
0.11[18]	8.47×10^{-8} - 7.06×10^{-7}	5

The experimental results of Uecker et al.[17] and Kokta et al.[8,18] are listed in Table 2. As calculated from equations (15), the differences in rotation rates do not change significantly the segregation coefficients. Therefore, these effective segregation coefficients of Ti are fitted as function of growth rate using equation (16). The fitting result gives the equilibrium segregation coefficient of Ti in sapphire to be $k_0 = 0.085 \pm 0.005$. It matches well with the reported values of k_0, 0.079 and 0.087, obtained from optical absorption measurement around seeding in sapphire doped with 0.5 wt.% Ti_2O_3 and 0.3 wt.% Ti_2O_3 and grown by the gradient freeze technique.[23] The fitted value is comparable to the thermodynamically calculated value $k_0 = 0.046$.

On one side, it is possible that, if the mismatch between Ti^{4+} solid solubility in the Al_2O_3 solid solution and the Al_2O_3-TiO_2 phase diagram could be further improved, the calculated k_0 value may be closer to the extrapolated experimental value. An attempt to adjust the solidus and liquidus lines in the phase diagram based on a private database from FactSage technical support with respect to the experimental data of Belon et al did not lead to an improved description.[42]

On the other side, strictly speaking, the fitted value $k_0 = 0.085$ is not the equilibrium segregation coefficient but the BPS equation fitted with the unrealistic $V_{\text{growth}} = 0$.[58] Since the BPS equation (15) always gives a $k_0 \leq k_{Ti}^{eff} \leq 1$, then the $k_0 = 0.085$ obtained from k_{Ti}^{eff} should be the threshold value. Therefore, both FactSage value 0.046 and fitted value 0.085 could be right. Consequently, a mean value of $k_0 = 0.06 \pm 0.02$ is proposed as the equilibrium segregation coefficient of Ti in

Ti:sapphire grown under reducing atmosphere.

Our calculated equilibrium segregation coefficient of Ti is much smaller than the effective segregation coefficient reported in Table 1 except the result of Fielitz et al. Their small value could be caused by large rotation rate which increases the homogeneity of solute in the melt, leading to effective segregation coefficient close to the equilibrium segregation coefficient. From the experimental data in Table 1, [12,15] it is noticed that Ti:sapphire grown by heat exchanger and Kyropolous methods with Mo crucible under vacuum or reducing atmosphere usually give a high effective segregation coefficient around 0.2 and high FOM values, i.e. high concentration ratio of Ti^{3+}/Ti^{4+}.

5 Conclusion

The thermodynamic database of the solid phases in the Al_2O_3-TiO_2 system is updated to study the influence of the oxygen partial pressure p_{O_2} on the Ti ion valence, Ti ion concentrations and segregation coefficients in the Al_2O_3 solid solution by referring to the experimental solid solubility limit of Ti^{3+} and Ti^{4+}. Through taking into account the effect of furnace gas, graphite heating elements and a Mo crucible, the calculation results show that the p_{O_2} partial pressure should not be lower than 10^{-20} bar during Ti:sapphire growth. In addition, the graphite elements show considerably more influence on p_{O_2} than the Mo crucible. By varying p_{O_2} at 2053 °C, it is found that the threshold oxygen partial pressure to obtain $[Ti^{3+}]_L > [Ti^{4+}]_L$ is $p_{O_2} < 10^{-7}$ bar and the threshold oxygen partial pressure to obtain $[Ti^{3+}]_S > [Ti^{4+}]_S$ is $p_{O_2} < 10^{-4}$ bar.

From the calculated Ti ion concentrations in the solid and liquid phases, the thermodynamic equilibrium segregation coefficients of Ti^{3+} and Ti^{4+} in Ti:sapphire are computed to be $k_{Ti^{3+}} = 0.046$ and $k_{Ti^{4+}} = 0.011$. A formula is derived in order to calculate the decrease of k_{Ti} from $k_{Ti^{3+}}$ to $k_{Ti^{4+}}$ as function of the increase of p_{O_2}.

Taking into account extrapolation of experimental effective segregation coefficients, a value of $k_0 = 0.06 \pm 0.02$ is proposed for the equilibrium segregation coefficient of Ti in Ti:sapphire under reducing atmosphere.

These results will be used for a proper resolution of the model of Ti^{3+} and Ti^{4+} distributions in Ti:sapphire after growth, as described in previous results.[59]

Acknowledgments

The technical support of Dr. Tatjana Jantzen and Dr. Joao Rezende from the FactSage company is warmly acknowledged. L. Xuan's PhD thesis was grant funded by the China Scholarship Council.

References

(1) Moulton, P. F. Spectroscopic and Laser Characteristics of Ti:Al_2O_3. *J. Opt. Soc. Am. B* **1986**, *3* (1), 125-133.

(2) Spence, D. E.; Kean, P. N.; Sibbett, W. 60-fsec Pulse Generation from a Self-Mode-Locked Ti:Sapphire Laser. *Opt. Lett.* **1991**, *16* (1), 42–44.

(3) Wall, K. F.; Schulz, P. A.; Aggarwal, R. L.; Lacovara, P.; Sanchez, A. A Ti:Al $_2O_3$/Master-Oscillator/Power-Amplifier System. *IEEE J. Quantum Electron.* **1993**, *29* (6), 1505–1514.

(4) McKinnie, I. T.; Oien, A. M. L.; Warrington, D. M.; Tonga, P. N.; Gloster, L. A. W.; King, T. A. Ti^{3+} Ion Concentration and Ti:Sapphire Laser Performance. *IEEE J. Quantum Electron.* **1997**, *33* (7), 1221–1230.

(5) Aggarwal, R. L.; Sanchez, A.; Stuppi, M. M.; Fahey, R. E.; Strauss, A. J.;

Rapoport, W. R.; Khattak, C. P. Residual Infrared Absorption in As-Grown and Annealed Crystals of Ti: Al_2O_3. *IEEE J. Quantum Electron.* **1988**, *24* (6), 1003–1008.

(6) Alombert-Goget, G.; Sen, G.; Pezzani, C.; Barthalay, N.; Duffar, T.; Lebbou, K. Large Ti-Doped Sapphire Single Crystals Grown by the Kyropoulos Technique for Petawatt Power Laser Application. *Opt. Mater. (Amst).* **2016**, *61*, 21–24.

(7) Evans, B. D.; Stapelbroek, M. Optical Properties of the F^+ Center in Crystalline Al_2O_3. *Phys. Rev. B* **1978**, *18* (12), 7089–7098.

(8) Kokta, M. R. Effects of Growth Conditions and Post-Growth Thermal Treatment on the Quality of Titanium-Doped Sapphire. In *Tunable Solid-State Lasers II*; Springer, 1986; pp 89–93.

(9) FactSage https://factsage.com/.

(10) Thermo-Calc https://thermocalc.com/.

(11) Pandat https://computherm.com/software.

(12) Ning, K.; Liu, Y.; Ma, J.; Zhang, L.; Liang, X.; Tang, D.; Li, R.; Hang, Y. Growth and Characterization of Large-Scale Ti:Sapphire Crystal Using Heat Exchange Method for Ultra-Fast Ultra-High-Power Lasers. *CrystEngComm* **2015**, *17* (14), 2801–2805.

(13) Schmid, F.; Khattak, C. P. Growth of Co: MgF_2 and Ti: Al_2O_3 Grystals for Solid State Laser Applications. In *Tunable Solid State Lasers*; Springer, 1985; pp 122–128.

(14) Nehari, A.; Brenier, A.; Panzer, G.; Lebbou, K.; Godfroy, J.; Labor, S.; Legal,

H.; Chériaux, G.; Chambaret, J. P.; Duffar, T.; Moncorgé, R. Ti-Doped Sapphire (Al_2O_3) Single Crystals Grown by the Kyropoulos Technique and Optical Characterizations. *Cryst. Growth Des.* **2011**, *11* (2), 445–448.

(15) Hu, K. Y.; Xu, J.; Wang, C. Y.; Li, H. J.; Zou, Y. Q.; Yang, Q. H. Study on Properties of Ti:Sapphire Crystals Doped Carbon Grown by the Kyropoulos Technique(KY). *Wuji Cailiao Xuebao.* **2012**, *27* (12), 1321–1324.

(16) Boulon, G. Fifty Years of Advances in Solid-State Laser Materials. *Opt. Mater. (Amst).* **2012**, *34* (3), 499–512.

(17) Uecker, R.; Klimm, D.; Ganschow, S.; Reiche, P.; Bertram, R.; Roßberg, M.; Fornari, R. Czochralski Growth of Ti:Sapphire Laser Crystals. *Opt. Based Biol. Chem. Sensing, Opt. Based Mater. Def.* **2005**, *5990*, 599006.

(18) Kokta, M. Growth of New Laser Crystals. In *Tunable Solid State Lasers for Remote Sensing*; Springer, 1985; pp 121–122.

(19) Fielitz, P.; Borchardt, G.; Ganschow, S.; Bertram, R.; Markwitz, A. 26Al Tracer Diffusion in Titanium Doped Single Crystalline α-Al_2O_3. *Solid State Ionics* **2008**, *179* (11–12), 373–379.

(20) Kimura, S.; Kitamura, K. Growth of Oxide Crystals for Optical Applications. *J. Ceram. Soc. Japan* **1993**, *101* (1169), 22–37.

(21) Nehari, A.; Duffar, T.; Ghezal, E. A.; Lebbou, K. Chemical Segregation of Titanium in Sapphire Single Crystals Grown by Micro-Pulling-down Technique: Analytical Model and Experiments. *Cryst. Growth Des.* **2014**, *14* (12), 6492–6496.

(22) Kimura, S.; Segawa, Y.; Kodama, N.; Kitamura, K.; Kosuda, K.; Tsutsumi, M. FZ Growth of Ti^{3+}: Al_2O_3 and Its Properties. In *New Slab and Solid-State Laser Technologies and Applications*; International Society for Optics and Photonics, 1987; Vol. 736, pp 29–33.

(23) Strauss, A. J.; Fahey, R. E.; Sanchez, A.; Aggarwal, R. L. Growth and Characterization of Ti:Al_2O_3 Crystals for Laser Applications. In *Laser and Nonlinear Optical Materials*; International Society for Optics and Photonics, 1987; Vol. 681, pp 62–71.

(24) Nizhankovskiy, S. V.; Dan'Ko, A. Y.; Krivonosov, E. V.; Puzikov, V. M. Growth of Large Ti:Sapphire Crystals by Horizontal Directional Solidification in Argon Atmosphere. *Inorg. Mater.* **2010**, *46* (1), 35–37.

(25) Nizhankovskiy, S. V.; Krivonosov, E. V.; Baranov, V. V; Budnikov, A. T.; Kanishchev, V. N.; Adonkin, G. T. Optical Homogeneity of Ti:Sapphire Crystals Grown by Horizontal Directional Solidification. *Inorg. Mater.* **2012**, *48* (11), 1111–1114.

(26) Dong, J.; Deng, P. Reply to Comments on "Ti:Sapphire Crystal Used in Ultrafast Lasers and Amplifiers." *J. Cryst. Growth* **2004**, *269* (2–4), 641–642.

(27) Kokta, M. R. Growth of Crystals for Solid State Lasers. In *Tunable Solid State Lasers*; Springer, **1985**; pp 105–114.

(28) Kokta, M. Growth of Oxide Laser Crystals. *Opt. Mater. (Amst).* **2007**, *30* (1), 1–5.

(29) Dean McKee JR, W.; Aleshin, E. Aluminum Oxide-titanium Oxide Solid

Solution. *J. Am. Ceram. Soc.* **1963**, *46* (1), 54–58.

(30) Yasuda, A.; Aoki, J.; Sakuma, T. Nanoprecipitation in Al_2O_3–3 mol% Ti_2O_3 Due to Oxidation. *Ceram. Int.* **1998**, *24* (7), 483–487.

(31) Ohta, M.; Morita, K. Thermodynamics of the Al_2O_3–SiO_2–TiO_X Oxide System at 1 873 K. *ISIJ Int.* **2002**, *42* (5), 474–481.

(32) Keig, G. A. Influence of the Valence State of Added Impurity Ions on the Observed Color in Doped Aluminum Oxide Single Crystals. *J. Cryst. Growth* **1968**, *2* (6), 356–360.

(33) Haneda, H.; Monty, C. Oxygen Self-diffusion in Magnesium-or Titanium-doped Alumina Single Crystals. *J. Am. Ceram. Soc.* **1989**, *72* (7), 1153–1157.

(34) Winkler, E. R.; Sarver, J. F.; Cutler, I. B. Solid Solution of Titanium Dioxide in Aluminum Oxide. *J. Am. Ceram. Soc.* **1966**, *49* (12), 634–637.

(35) Burdick, J. N. United States Patent Office ,Synthetic Star Rubies and Star Sapphires, and Process for Producing Same. **1949**, 3–5.

(36) Bagley, R. D.; Cutler, I. B.; Johnson, D. L. Effect of TiO_2 on Initial Sintering of Al_2O_3. *J. Am. Ceram. Soc.* **1970**, *53* (3), 136–141.

(37) Hwang, C.-S.; Nakagawa, Z.; Hamano, K. Microstructure and Mechanical Strength of TiO_2-Doped Al_2O_3 Ceramics Fired in Vacuum Atmosphere. *J. Ceram. Soc. Japan* **1993**, *101* (1177), 1051–1056.

(38) Hamano, K. Effects of TiO_2 on Sintering of Alumina Ceramics. *J. Ceram. Soc. Japan* **1986**, *94* (5), 505.

(39) Petot-Ervas, G.; Saadi, B.; Petot, C.; Loudjani, M. Transport Properties of

Titanium-Doped α-Alumina: Experimental Results. *J. Eur. Ceram. Soc.* **1997**, *17* (7), 943–950.

(40) Roy, S. K.; Coble, R. L. Solubilities of Magnesia, Titania, and Magnesium Titanate in Aluminum Oxide. *J. Am. Ceram. Soc.* **1968**, *51* (1), 1–6.

(41) Horibe, T.; Yamada, H.; Katto, S. Changes of Surface Morphology of Titanium (III)-Containing Corundum by Heating in Air. *J. Ceram. Assoc. Japan* **1969**, *77* (886), 187–193.

(42) Belon, L.; Forestier, H. Study of the System Al_2O_3-Ti_2O_3(Formation of Eutectic Mixture of Titanium Oxide-Aluminum Oxide System with a Particular Solubility Limit). *Comptes Rendus* **1964**, *258* (17), 4282–4284.

(43) Eriksson, G.; Pelton, A. D. Critical Evaluation and Optimization of the Thermodynamic Properties and Phase Diagrams of the MnO-TiO_2, MgO-TiO_2, FeO-TiO_2, Ti_2O_3-TiO_2, Na_2O-TiO_2, and K_2O-TiO_2 Systems. *Metall. Trans. B* **1993**, *24* (5), 795–805.

(44) Stelian, C.; Alombert-Goget, G.; Sen, G.; Barthalay, N.; Lebbou, K.; Duffar, T. Interface Effect on Titanium Distribution during Ti-Doped Sapphire Crystals Grown by the Kyropoulos Method. *Opt. Mater. (Amst).* **2017**, *69*, 73–80.

(45) Lacovara, P.; Esterowitz, L.; Kokta, M. Growth, Spectroscopy, and Lasing of Titanium-Doped Sapphire. *IEEE J. Quantum Electron.* **1985**, *21* (10), 1614–1618.

(46) Deng, P.; Chai, Y.; Yan, S.; Zhang, G.; Sun, Y.; Gan, F. Investigation on Improvement of Laser Quality of Tunable Al_2O_3:Ti^{3+} Crystals. *Optoelectron.*

Devices Appl. **1990**, *1338* (November 1990), 207.

(47) Sidelnikova, N. S.; Nizhankovskyi, S. V.; Baranov, V. V. Charge State of the Activator in Ti:Sapphire Crystals Grown by HDC Method. *Functional Materials*. 2015, pp 271–279.

(48) Borodin, V. A.; Steriopolo, T. A.; Tatarchenko, V. A.; Chernyshova, L. I.; Yalovets, T. N. Production of Sapphire Tubes for High-pressure Sodium Lamps Using the Stepanov Method at High Rates of Growth. *Cryst. Res. Technol.* **1985**, *20* (2), 159–166.

(49) Wendel, J. Thermodynamics and Kinetics of Tungsten Oxidation and Tungsten Oxide Sublimation in the Temperature Interval 200–1100 C. *Diploma Work* **2014**.

(50) S. K. Mohapatra, K. F. A. Defect Structure of α-Al_2O_3 Doped with Titanium. *J. Am. Ceram. Soc.* **1977**, *60*, 381−387.

(51) Nizhankovskii, S. V.; Sidel'nikova, N. S.; Baranov, V. V. Optical Absorption and Color Centers in Large Ti:Sapphire Crystals Grown by Horizontally Directed Crystallization under Reducing Conditions. *Phys. Solid State* **2015**, *57* (4), 781–786.

(52) Moskvin, N. A., Sandulenko, V. A., Sidorova, E. A. Color Centers and Luminescence in Corundum Crystals Containing Titanium. *J. Appl. Spectrosc.* **1980**, *32* (6), 592–596.

(53) Dess, H. M. Melt Growth of Refractory Oxide Single Crystals. In *Crystallization from solutions and melts*; Springer, **1969**; pp 100–111.

(54) Burton, J. A.; Prim, R. C.; Slichter, W. P. The Distribution of Solute in Crystals Grown from the Melt. Part I. Theoretical. *J. Chem. Phys.* **1953**, *21* (11), 1987–1991.

(55) Burton, J. A.; Kolb, E. D.; Slichter, W. P.; Struthers, J. D. Distribution of Solute in Crystals Grown from the Melt. Part II. Experimental. *J. Chem. Phys.* **1953**, *21* (11), 1991–1996.

(56) Wenjia, S.; Duffar, T.; Nehari, A.; Kononets, V.; Lebbou, K. Modeling of Dopant Segregation in Sapphire Single Crystal Fibre Growth by Micro-Pulling-down Method. *J. Cryst. Growth* **2017**, *474*, 43–49.

(57) D. Klim, So. Ganschow, private communication, June **2020**.

(58) Müller, G. Convection and Inhomogeneities in Crystal Growth from the Melt. In *Crystal Growth from the Melt*; Springer, **1988**; pp 1–136.

(59) Xuan, L.; Duffar, T. Physico-Chemical Model for Dopant Charge State Conversion during Ti:Sapphire Crystal Growth. *J. Cryst. Growth* **2021**, *570*, 126234.

For Table of Contents Use Only

Title: Thermodynamic Calculations of Ti Ion Concentrations and Segregation Coefficients During Ti:sapphire Crystal Growth

Authors: Lingling Xuan[a], Alexander Pisch[a], Thierry Duffar[a*]

[a]*Univ. Grenoble Alpes, CNRS, Grenoble INP, SIMAP, 38000 Grenoble, France*

**E-mail: thierry.duffar@grenoble-inp.fr*

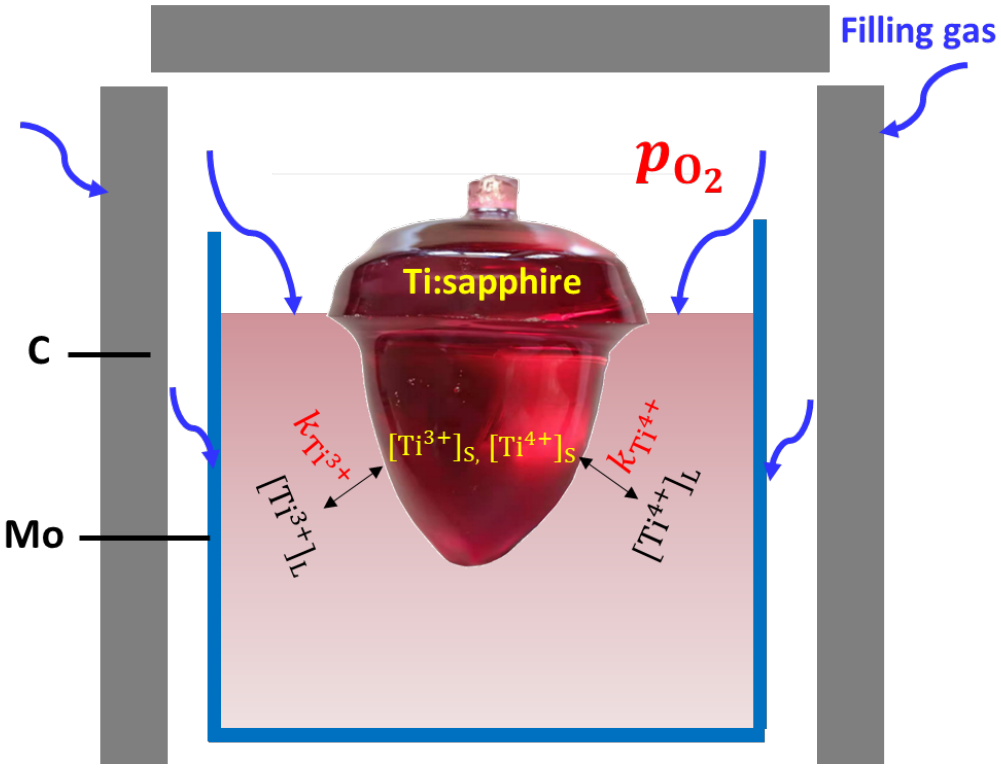

The influence filling gas on graphite elements and Mo crucible on p_{O_2} thereby the concentration of Ti^{3+} and Ti^{4+} in the solid and liquid phases and their segregation coefficients during Ti:sapphire growth process.